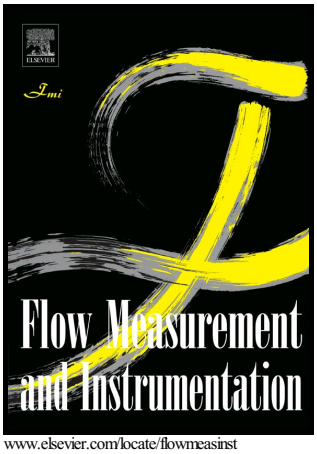

www.elsevier.com/locate/flowmeasinst

Monitoring a Francis Turbine Operating Conditions

P. João Gomes, Loïc Andolfatto, François Avellan

PII: S0955-5986(18)30239-5
DOI: https://doi.org/10.1016/j.flowmeasinst.2018.07.007
Reference: JFMI1462

To appear in: *Flow Measurement and Instrumentation*

Received date: 20 June 2018
Accepted date: 27 July 2018

Cite this article as: P. João Gomes, Loïc Andolfatto and François Avellan, Monitoring a Francis Turbine Operating Conditions, *Flow Measurement and Instrumentation,* https://doi.org/10.1016/j.flowmeasinst.2018.07.007

Monitoring a Francis Turbine Operating Conditions

João Gomes P. Jr.[a,1,*], Loïc Andolfatto[a,1], François Avellan[a,1]

[a] *Av. du Cour 33 bis, 1004 Lausanne, Switzerland*

Abstract

Francis turbines are designed for a specific set of operating conditions that is particular to each hydropower plant site. It allows this type of turbine to extract as much hydraulic power as possible, as long as they are operating in the right conditions. For this reason, power plant operators must know in advance what are the best conditions for operating their generating units and, naturally, in which exact conditions these units are actually operating. Detailed information about the turbine behavior in any operating condition can be obtained by performing measurements in a reduced scale physical model of the turbine prototype. These tests provide what is known as the turbine hill chart: a two-dimensional graphical representation of the most relevant turbine properties showing, for instance, the power output, the discharge, the efficiency and the cavitation conditions. This paper presents a method to monitor the operating conditions of a Francis turbine by locating it on the hill chart. To do so, it requires the generation of polynomial bi-variate functions based on Hermite polynomials that can calculate the turbine discharge and efficiency from its guide vanes angle and power output. A test case is presented with a turbine prototype of 444 MW of rated power operating through a wide range of operating conditions. The validation is done by comparisons between the measured and estimated values of gross head, leading to similar values.

Keywords: Francis turbine, Operating conditions, Hermite polynomials,

*Corresponding author

Email addresses: joao.gomes@epfl.ch (João Gomes P. Jr.), loic.andolfatto@epfl.ch (Loïc Andolfatto), francois.avellan@epfl.ch (François Avellan)

[1] Laboratory for Hydraulic Machines, EPFL

1. Introduction

Hydraulic turbines are required to operate in a wide range of conditions and to adjust its power output to the variations of water availability, energy demand and energy generation from other resources. Depending on factors such as the available specific energy and discharge, the turbine may operate in non-optimal conditions, affecting their performance and shortening their lifespan.

Francis turbines feature fixed blades, preventing them to better adapt to available energy and discharge variations, resulting in efficiency loss and the generation of a vortex swirling flow at part load conditions [1] and full load conditions [2]. Additionally, cavitation may happen when the counter-pressure provided by the downstream reservoir water level is low. This cavitation can cause pressure pulsations and induce wear and tear and vibration, increasing the risk of failure as discussed in [3] and [4]. General information about cavitation generation and its impacts in a Francis turbine can be found in [5], [6] and [7].

To mitigate the drawbacks of these harsh operating conditions and to optimize the exploitation of generating units containing Francis turbines, two different steps are required. The first step is to investigate how the machine behaves in every possible operating condition of interest, generating a picture that is unique for each turbine design. The second step is to monitor online, through measurements, where exactly inside this larger picture the turbine is actually operating.

This general picture is known as the turbine hill chart. It provides all the necessary information regarding efficiency, cavitation, vortex-rope presence and power generation, for instance. The complete hill chart of a turbine prototype can be obtained through measurements on a homologous reduced scale model using a test rig specially designed for this purpose. Measurements on the reduced scale physical model are performed with a high level of accuracy that usually cannot be achieved in the prototype.

This paper proposes then a monitoring system technique based in this two steps approach. It takes only two direct measurements on the prototype to estimate in what conditions, inside the hill chart, the turbine is operating. For the generation of the complete hill chart, it requires continuous functions to interpolate the measurements on the scaled model. These functions are generated through a combination of Hermite polynomials and modal strengths.

The proposed monitoring technique differs from others like the one presented by Valero et al. [8], as it is focused on physical quantities that can be transposed, such as the discharge and the efficiency. For its simplicity, it can make it easier to put into practice plant optimization models as those proposed by [9], [10] and [11].

A test case is presented where the methodology is applied and the operating conditions are estimated. For the validation, calculated values of gross head are compared with measurements showing good agreement. The results obtained suggest us that the methodology can provide reliable online estimations of the operating conditions of the prototype.

2. Model tests and hill chart generation

Performing tests on reduced scale physical model of hydraulic turbines is a mandatory phase for the most important hydropower projects as it provides detailed information on the turbine that cannot be accurately calculated. These tests are performed in accordance with the IEC standard [12], where the procedures to assure a high level of measurements accuracy and the general rules to transpose the results from the model to the prototype scale are presented. The IEC standard [13] also proposes transposition procedures, but in a more refined manner as it takes into account, for instance, the differences of surface roughness between model and prototype.

To simplify comparisons between homologous turbines with different diameters and rotating speeds, the IEC standard propose the use of non-dimensional

discharge and speed factors, Q_{ED} and n_{ED} respectively. They are defined as:

$$Q_{\mathrm{ED}} = \frac{Q}{D^2\sqrt{E}} \qquad n_{\mathrm{ED}} = \frac{nD}{\sqrt{E}} \qquad E = gH \tag{1}$$

where Q is the discharge, D is the turbine reference diameter, n is the runner rotation frequency, E is the turbine specific energy, g is the local gravity acceleration and H is the turbine head.

All these measurements and non-dimensional factors can then be used to generate the turbine hill chart. A turbine hill chart can be considered as a dashboard where the plant operator can catch at a glance a great number of relevant information about the turbine and decide in which conditions the turbine is supposed to operate.

An example of hill chart having Q_{ED} and n_{ED} in its x and y axes is presented in Figure 1. This hill chart contains measurements that were performed in a reduced scale model from where all the data is interpolated to create the isolines and zones that are shown. It presents isolines of turbine hydraulic efficiency η, guide vanes opening angle α and mechanical power provided by the turbine P_{m}. It also presents the best efficiency point (BEP) and four different zones:

- The inlet cavitation zone, corresponding to the rated level of the downstream reservoir;
- The interblade cavitation (see [14]), also corresponding to the rated level of the downstream reservoir;
- The rated operating zone where the turbine must operate according to the specifications;
- The vortex rope-free zone.

The hydraulic efficiency and mechanical power are defined as in Equation 2. The values shown in this hill chart are already transposed to the prototype scale.

$$\eta = \frac{P_{\mathrm{m}}}{P_{\mathrm{H}}} \qquad P_{\mathrm{m}} = P_{\mathrm{H}} - P_{\mathrm{LT}} \qquad P_{\mathrm{H}} = \rho Q E \tag{2}$$

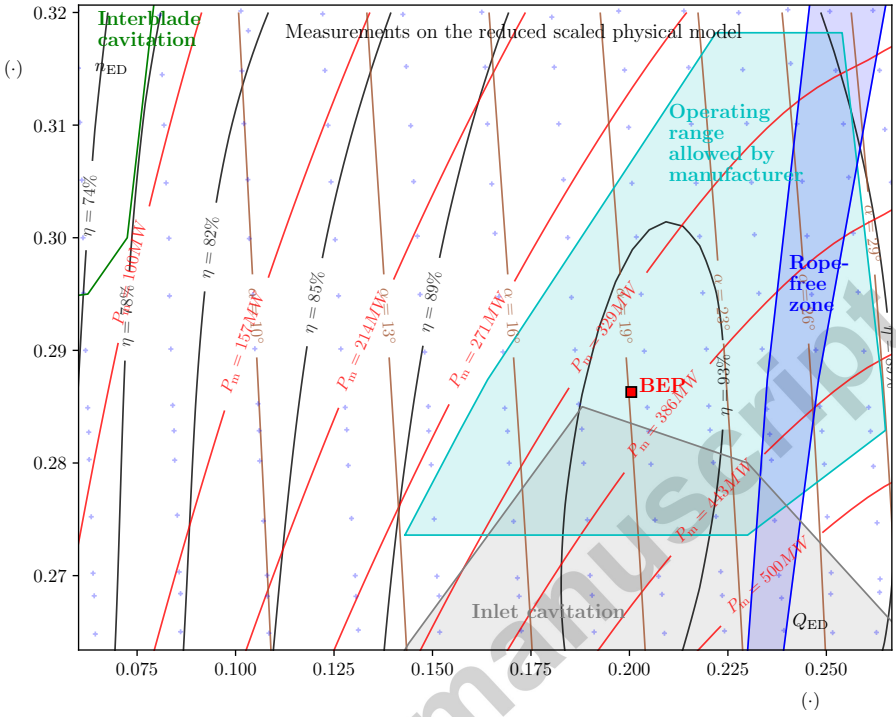

Figure 1: Example of the Q_{ED}, n_{ED} hill chart featuring efficiency isolines, the BEP, the operating range, the rope-free and cavitation zones limits of a Francis turbine.

where P_H is the hydraulic power and P_{LT} is the sum of the power losses inside the turbine, combining the specific hydraulic energy loss, the leakage flow loss and the disc friction power loss.

3. Hermite polynomials interpolation method

The measurements on the reduced scale physical model provide information only on a finite number of points of the complete hill chart. An interpolation method is then required to cover the complete range where the turbine operates.

It is assumed that any variable of interest, such as the discharge or the efficiency, can be represented through a continuous bivariate function covering all this domain of possible operating conditions. With this assumption, the Weierstrass approximation theorem can be used [15]. This theorem states that every

continuous function defined on a closed interval can be uniformly approximated by a polynomial surrogate function. Therefore, this paper uses surrogate functions that are generated as a combination of Hermite polynomials [16], similarly to the methodology proposed by Andolfatto et al in [17].

The Hermite polynomials $He_{n,m}$, with $n, m \in \mathbb{N}$, form a complete basis of functions inside the Hilbert space that are orthogonal with respect to the scalar product defined as:

$$\left\langle He_{i,j}, He_{k,l} \right\rangle = \int_{\mathbb{R}^2} He_{i,j}\left(\mathbf{X}\right) \cdot He_{k,l}\left(\mathbf{X}\right) \cdot \frac{1}{2\pi} \exp\left(-\frac{\mathbf{X}^2}{2}\right) d\mathbf{X} \tag{3}$$

with $\mathbb{R}$ being the set of real numbers, $\mathbf{X}$ being an input vector, $He_{i,j}$ and $He_{k,l}$ being any Hermite polynomial.

Hermite polynomials can be recursively defined as:

$$\begin{cases} He_{n+1,1} = a_n \cdot X_1 \cdot He_{n,1} + b_n \cdot He_{n-1,1} \\ He_{n+1,m} = He_{m-1,m} \cdot He_{n-m+2,1} \\ He_{n+1,n+2} = a_n \cdot X_2 \cdot He_{n,n+1} + b_n \cdot He_{n-1,n} \end{cases} \tag{4}$$

With the boundary conditions:

$$\begin{gathered} He_{0,1} = 1 \qquad He_{1,1} = X_1 \qquad He_{1,2} = X_2 \\ a_n = \sqrt{\frac{1}{n+1}} \qquad b_n = -\sqrt{\frac{n}{n+1}} \qquad m \in [\![2, n+1]\!] \end{gathered} \tag{5}$$

where X_1 and X_2 are the input variables inside the vector $\mathbf{X}$. This definition for the Hermite polynomials is known as the probabilistic form of the family.

Each Hermite polynomial $He_{n,m}$ can be represented with only one index by applying the change from m, n to p as defined in Equation 6. The graphical representation of Hermite polynomials $\mathrm{He}_p = He_{n,m}$ with index p varying from zero to 14, corresponding to a fourth degree polynomial, is shown in Figure 2.

$$\begin{gathered} \mathrm{He}_{p \in \mathbb{N}} = He_{n,m} \\ \forall n \in \mathbb{N}, \forall m \in [\![1, n+1]\!], p = \frac{n(n+1)}{2} + m - 1 \end{gathered} \tag{6}$$

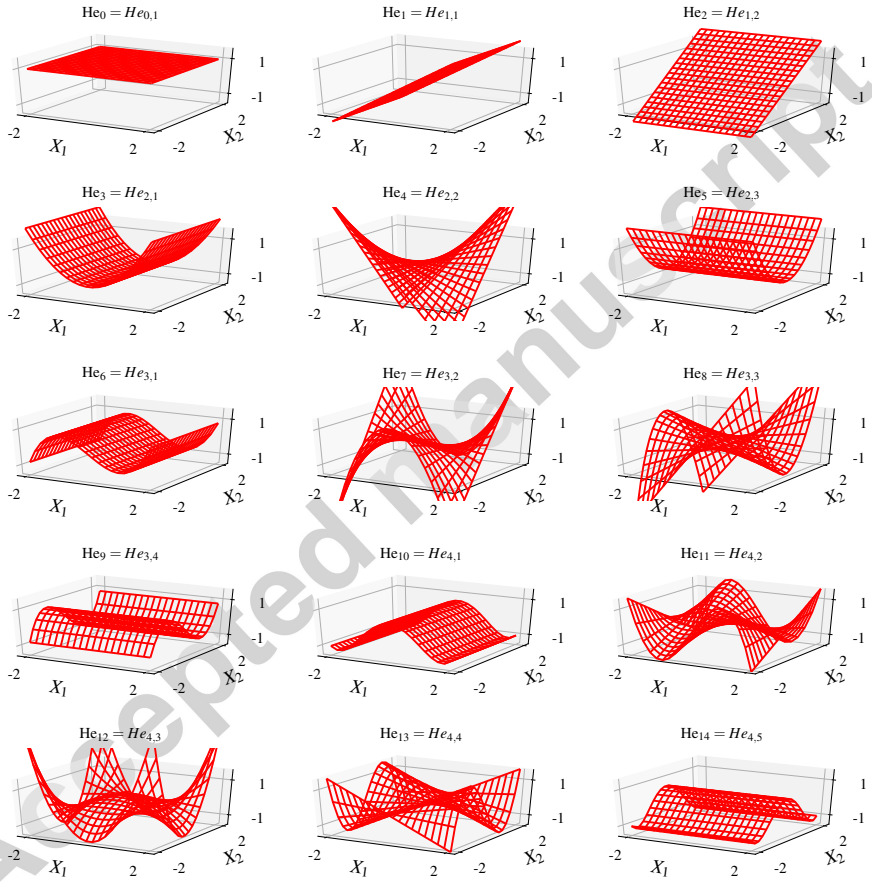

Figure 2: Graphical representation of Hermite polynomials with index p from zero to 14.

It is then possible to define surrogate functions in the form:

$$\hat{f} = \sum_{p=0}^{p_{\max}} \lambda_p \mathrm{He}_p(\mathbf{X}) \tag{7}$$

meaning that the surrogate function $\hat{f}$ approximates a given function f using only a truncated basis of Hermite polynomials. The truncation parameter $p_{\max}$ and the coefficients $\lambda_p \in \mathbb{R}$, known as the modal strengths, must be chosen properly aiming to minimize the deviations between the function $\hat{f}$ and its target function f.

The explicit form of the target function f is, for the case discussed in this paper, unknown. Although, it is assumed that the performed measurements provide points on the surface given by f. In this case, one way to define the vector $\boldsymbol{\lambda}$ containing the modal strengths and to minimize the error between $\hat{f}$ and f is by using the least-squares method. The vector of modal strengths is then defined as:

$$\boldsymbol{\lambda} = \begin{bmatrix} \lambda_1 & \lambda_2 & \dots & \lambda_{p_{\max}} \end{bmatrix}^T = \left(\mathbf{He}^T\mathbf{He}\right)^{-1}\mathbf{He}^T\mathbf{f} \tag{8}$$

where:

$$\mathbf{f} = \begin{bmatrix} {}^{(1)}f & {}^{(2)}f & \dots & {}^{(N_s)}f \end{bmatrix}^T \tag{9}$$

$$\mathbf{He} = \begin{bmatrix} \mathrm{He}_0\left({}^{(1)}\mathbf{X}\right) & \mathrm{He}_1\left({}^{(1)}\mathbf{X}\right) & \dots & \mathrm{He}_{p_{\max}}\left({}^{(1)}\mathbf{X}\right) \\ \mathrm{He}_0\left({}^{(2)}\mathbf{X}\right) & \mathrm{He}_1\left({}^{(2)}\mathbf{X}\right) & \dots & \mathrm{He}_{p_{\max}}\left({}^{(2)}\mathbf{X}\right) \\ \vdots & \vdots & \ddots & \vdots \\ \mathrm{He}_0\left({}^{(N_s)}\mathbf{X}\right) & \mathrm{He}_1\left({}^{(N_s)}\mathbf{X}\right) & \dots & \mathrm{He}_{p_{\max}}\left({}^{(N_s)}\mathbf{X}\right) \end{bmatrix} \tag{10}$$

and the superscript ${}^{(k)}\forall k \in [\![1, N_s]\!]$ indicates the number of the measurement sample and N_s is the total number of samples.

Hermite polynomials are defined with respect to a standard normal Gaussian distribution. For this reason, its input variables are expected to have zero mean, zero correlation between them and to remain mostly inside the interval $[-1, 1]$. These conditions are usually not fulfilled among the measurements that are

performed on the turbine. For this reason, a *transformation function* can be applied to map the measurements into a new set of variables that adapts better to these requirements.

As the modal strengths are calculated based only on the available measurement samples, the truncation parameter $p_{\max}$ must be chosen wisely to avoid polynomial approximations that either underfits or overfits the data. Underfitting happens when $p_{\max}$ is too low, leading to large deviations between the measurements and $\hat{f}$. Overfitting is observed when $p_{\max}$ is too high, reducing the error between $\hat{f}$ and the available measurements to a minimum, but leading to large deviations if points outside the original training set of points are evaluated.

There are different criteria that can help to identify a polynomial approximation that is underfitting or overfitting the training database. One of them is the Akaike Information Criterion (AIC) [18], that can be applied here as:

$$\mathrm{AIC} = N_s \left(\log \sigma^2 + 1 \right) + 2 \left(p_{\max} + 1 \right) \tag{11}$$

where σ^2 is the variance of the error inside the available points. As it can be seem in equation 11, the AIC will be high either if the model underfits the training data (high variance) or if it overfits the training data (high $p_{\max}$). Consequently, while comparing different $p_{\max}$ options for the same approximation, those with a good compromise between number of parameters and error will have a low AIC.

As the dimensionality of the approximation can sometimes be close to the number of available samples N_s, a correction for the AIC can be employed, as proposed in [19]. The corrected AIC, namely AICc, is employed in this paper as:

$$\mathrm{AICc} = \mathrm{AIC} + \frac{2 \left(p_{\max} + 1 \right) \left(p_{\max} + 2 \right)}{N_s - p_{\max} - 2} \tag{12}$$

4. Methodology

To find the exact location inside the hill chart where a Francis turbine prototype is operating, two measurements input are required. In any typical hydropower plant, the guide vanes angle α and the active power output from the generator P_{a} can be measured with accuracy and low cost. This pair of measurements is then proposed in this paper.

The guide vanes angle is not usually measured directly during a normal plant operation, but it can be easily obtained through kinematic relations between the guide vane opening angle and the servomotor stroke. Speed governors usually keep this parameter under constant monitoring.

Procedures to measure P_{a} are described in the IEC standard [20]. The relation between P_{a} and the mechanical power provided by the turbine P_{m} can be written as:

$$P_{\mathrm{a}} = P_{\mathrm{m}} - P_{\mathrm{LB}} - P_{\mathrm{LG}} \tag{13}$$

where P_{LB} includes the power losses in all the bearings and P_{LG} all the losses in the generator. These losses are usually calculated with precision by the manufacturers and they can be verified by the calorimetric method [21].

Assuming that the power losses are known, explicit relations between α, P_{a} and the remaining operating variables that are shown in the hill chart can be derived. For this purpose, surrogate functions as in Equation 7 can be generated and a transformation functions g_{T} can be defined to transform α and P_{a} into X_1 and X_2, the two terms of the input vector $\mathbf{X}$.

In this paper, two surrogate functions are chosen: one for the discharge, $\hat{f}_Q$, and another for the turbine efficiency, $\hat{f}_\eta$. The methodology to obtain the discharge Q and the efficiency η of the prototype is summarized in the diagram of Figure 3. The methodology can be divided in two main parts:

1. *identification procedure*: where the transformation function g_{T} and the surrogate functions $\hat{f}_Q$ and $\hat{f}_\eta$ are defined according to the measurements performed on the reduced scale physical model;

2. *exploitation procedure*: where the actual turbine prototype discharge and efficiency are estimated online from the generating unit α and P_{a}.

Once the prototype discharge and and efficiency are known:

- the turbine available specific energy E is calculated as:

$$E = \frac{P_{\mathrm{m}}}{\eta\rho Q} = \frac{P_{\mathrm{a}} + P_{\mathrm{LB}} + P_{\mathrm{LG}}}{\eta\rho Q} \tag{14}$$

- knowing that the rotating speed and diameter of the prototype are fixed, n_{ED} and Q_{ED} are calculated as in Equation 1;

5. Application

5.1. Test case description

The operating conditions of a Francis turbine prototype of IEC specific speed $n_{\mathrm{QE}} = 0.131$ (or $N_{\mathrm{q}} = NQ^{0.5}H^{-0.75} = 43.5$, where N is the rotation speed in min^{-1}) are estimated with the proposed monitoring methodology. Measurements on its homologous reduced scale physical model were performed previously, providing the data to build the hill chart of Figure 1.

The reduced scale physical model features a runner of 0.35 m diameter and the measurements were performed at 800 min^{-1} rotation speed. A total of $N_s = 329$ operating points were investigated, with guide vanes opening angle varying from 5° to 32°, covering any possible condition of interest for the prototype operations.

General information related to the generating unit containing the turbine prototype is presented in the Table 1. The local gravity g is calculated according to the IEC standard [20], based on the location of the turbine. Also according to [20], ρ is calculated based on the mean water temperature. Field acceptance tests performed previously yield an energy energy loss coefficient K defined as:

$$K = \left(gH_{\mathrm{g}} - E\right)\left(\frac{Q^2}{2A^2}\right)^{-1} \qquad A = \frac{\pi D^2}{4} \tag{15}$$

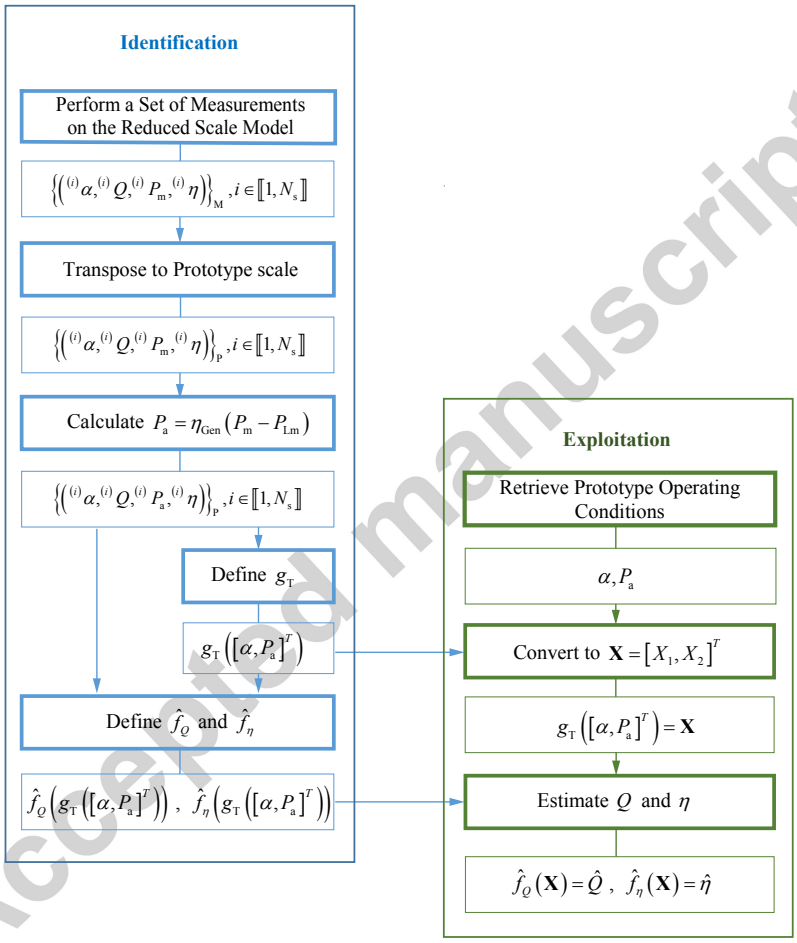

Figure 3: Procedure for the parameters identification and determination of the turbine prototype efficiency and discharge.

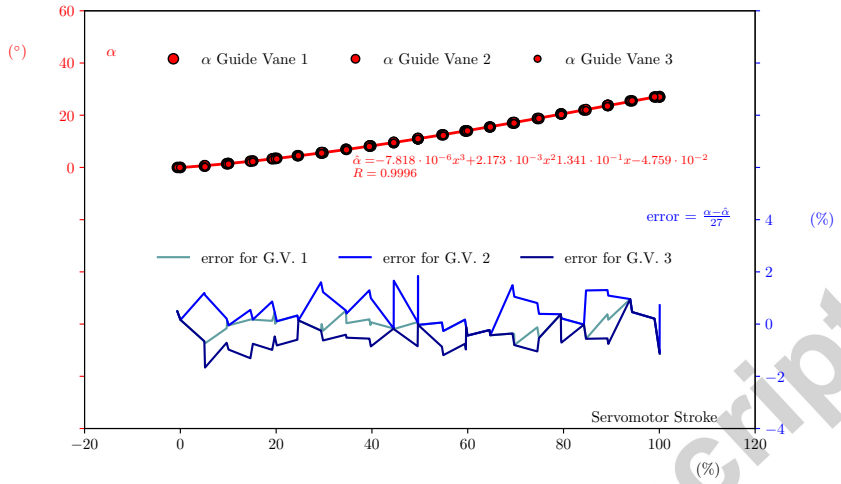

Figure 4: Calibration curve for the guide vane angle according to the servomotor stroke. Measurements are performed at three different guide vanes and the relative error between them and the best fit curve is also presented.

where gH_g is the specific potential energy of the power plant and H_g is the plant gross head equal to the difference between the headwater and the tailwater reservoir levels. The table also provides the generator efficiency η_{Gen}, allowing P_{LG} to be calculated as:

$$\eta_{Gen} = \frac{P_a}{P_m - P_{LB}} \qquad P_{LG} = P_a \left(\frac{1}{\eta_{Gen}} - 1 \right) \tag{16}$$

The calibration curve of the guide vane angle as a function of the servomotor stroke is presented in Figure 4. The guide vane angle of three different guide vanes is measured and a best fit polynomial curve is generated. The error between the measurements and the best fit curve is also shown in Figure 4.

A total of 17 measurements were performed at different operating conditions on the prototype. Each measurement is performed after the stabilization of the temperature of the bearings and keeping a constant guide vanes opening during approximately 6 minutes for each operating condition. The guide vanes opening angle, the active output power from the generator and the plant gross head were constantly recorded. The downstream reservoir remained close to the rated level,

Table 1: Test case data of the prototype generating unit.

Rated active power output	P_{Rated}	443.7 MW
Rated head	H_{Rated}	170.7 mwc
Rated discharge	Q_{Rated}	288 $\text{m}^3\cdot\text{s}^{-1}$
Rotation speed	N_{Proto}	128.6 min^{-1}
Reference diameter	D_{Proto}	5.4 m
Generator efficiency[a]	η_{Gen}	98.5 %
Bearing losses[a]	P_{LB}	350 kW
Local gravity[b]	g	9.8096 $\text{m}\cdot\text{s}^{-1}$
Water density[b]	ρ	999.92 $\text{kg}\cdot\text{m}^{-3}$
Energy loss coefficient[c]	K	0.156

[a] Estimated values.

[b] According to (International Electrotechnical Commission, 1991).

[c] Estimative based on previous tests on this generating unit.

keeping the cavitation properties as in Figure 1.

5.2. The transformation function

The transformation function g_{T} described in Equation 17 transforms the opening angles α and the active power P_{a} into the input variables for the Hermite polynomials X_1 and X_2. It performs a translation and a normalization of both α and P_{a}, whereas the translation and normalization parameters for P_{a} requires knowing its related α value.

$$g_{\text{T}}\left(\begin{bmatrix}\alpha\\ P_{\text{a}}\end{bmatrix}\right) = \underbrace{\begin{bmatrix}\frac{2}{\alpha_{\max}-\alpha_{\min}} & 0\\ 0 & \frac{2}{\text{UP}(\alpha)-\text{LP}(\alpha)}\end{bmatrix}}_{\text{Normalization}}\underbrace{\begin{bmatrix}\alpha-\overline{\alpha}\\ P_{\text{a}}-\overline{P}_{\text{a}}(\alpha)\end{bmatrix}}_{\text{Translation}} = \begin{bmatrix}X_1\\ X_2\end{bmatrix} \tag{17}$$

where $\alpha_{\min}$ is the minimum guide vanes opening inside the database of measurements performed in the reduced scale physical model, $\alpha_{\max}$ is the maximum value and $\overline{\alpha}$ is the mean value between $\alpha_{\min}$ and $\alpha_{\max}$.

The functions $\text{LP}(\alpha)$ and $\text{UP}(\alpha)$ are third degree polynomial functions that best fits, respectively, the lowest and the highest values of P_{a} according to the

Table 2: Mean, standard deviation and correlation of the input variables

	$\alpha\,(^\circ)$	$P_\mathrm{a}\,(\mathrm{MW})$	$X_1\,(\cdot)$	$X_2\,(\cdot)$
Mean	18.05	311.31	0.00	-0.29
Standard deviation	8.36	182.12	0.62	0.50
Correlation coefficient	$\mathrm{corr}\,(\alpha, P_\mathrm{a}) = 0.70$		$\mathrm{corr}\,(X_1, X_2) = 0.04$	

tested opening angle α. Their coefficients are defined by minimizing L_LP and L_UP defined as:

$$L_\mathrm{LP} = \sum_{k=1}^{N_s} {}^{(k)}W_\mathrm{LP}\left({}^{(k)}P_\mathrm{a} - \mathrm{LP}\left({}^{(k)}\alpha\right)\right)^2 \tag{18}$$

$$L_\mathrm{UP} = \sum_{k=1}^{N_s} {}^{(k)}W_\mathrm{UP}\left({}^{(k)}P_\mathrm{a} - \mathrm{UP}\left({}^{(k)}\alpha\right)\right)^2 \tag{19}$$

where:

$${}^{(k)}W_\mathrm{LP} = \begin{cases} 1, \text{ if } {}^{(k)}P_\mathrm{a} - \mathrm{LP}\left({}^{(k)}\alpha\right) > 0 \\ 10^4, \text{ if } {}^{(k)}P_\mathrm{a} - \mathrm{LP}\left({}^{(k)}\alpha\right) \leq 0 \end{cases} \tag{20}$$

$${}^{(k)}W_\mathrm{UP} = \begin{cases} 10^4, \text{ if } {}^{(k)}P_\mathrm{a} - \mathrm{UP}\left({}^{(k)}\alpha\right) > 0 \\ 1, \text{ if } {}^{(k)}P_\mathrm{a} - \mathrm{UP}\left({}^{(k)}\alpha\right) \leq 0 \end{cases} \tag{21}$$

Finally, the function $\overline{P}_\mathrm{a}\,(\alpha)$ is a moving average for P_a, calculated as:

$$\overline{P}_\mathrm{a}\,(\alpha) = \frac{\mathrm{UP}\,(\alpha) + \mathrm{LP}\,(\alpha)}{2} \tag{22}$$

The resulting transformation of the N_s values of α and P_a into the transformed variables X_1 and X_2 is shown in Figure 5. The mean and the standard deviation values of both the original and transformed variables are presented in the table 2. Additionally, the correlation between α and P_a and the correlation between X_1 and X_2 is also given. The presented values confirm that X_1 and X_2 are in agreement with the conditions where the Hermite Polynomials are defined.

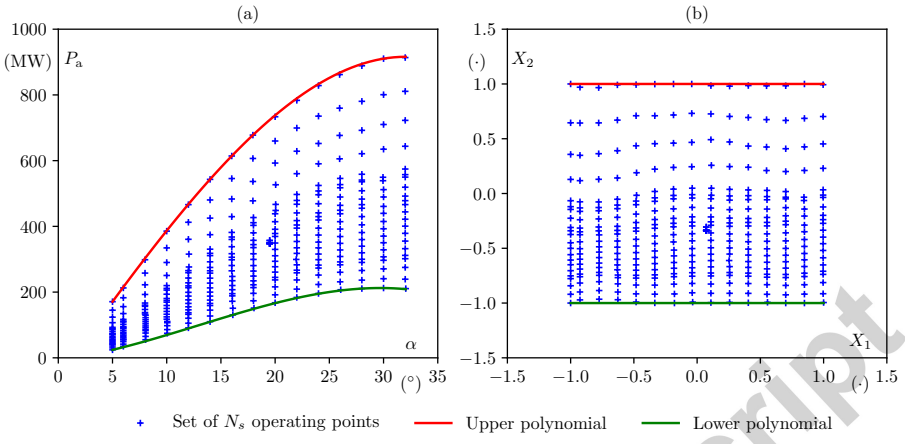

Figure 5: (a) The values of α and P_a for the N_s operating points tested on the model. (b) Corresponding values of the transformed variables X_1 and X_2.

5.3. Surrogate functions for the discharge and efficiency

By applying the methodology for the generation of surrogate functions, the discharge function $\hat{f}_Q$ and the turbine efficiency function $\hat{f}_\eta$ can be defined as:

$$\hat{f}_Q(\alpha, P_a) = \sum_{p=0}^{p_{Q\max}} \lambda_{Q_p} \mathrm{He}_p(g_T(\alpha, P_a)) = \sum_{p=0}^{p_{Q\max}} \lambda_{Q_p} \mathrm{He}_p(\mathbf{X}) = \hat{Q} \tag{23}$$

$$\hat{f}_\eta(\alpha, P_a) = \sum_{p=0}^{p_{\eta\max}} \lambda_{\eta_p} \mathrm{He}_p(g_T(\alpha, P_a)) = \sum_{p=0}^{p_{\eta\max}} \lambda_{\eta_p} \mathrm{He}_p(\mathbf{X}) = \hat{\eta} \tag{24}$$

where $\hat{Q}$ and $\hat{\eta}$ are the estimated values for the prototype discharge and efficiency, respectively.

Possible values for the truncation parameters $p_{Q\max}$ and $p_{\eta\max}$ varying from 3 to 135 are evaluated and their AICc, maximum absolute error, mean absolute error and standard error are presented in Figure 6(a) and Figure 7(a). For both discharge and efficiency, the surrogate functions with the lowest truncation parameter values present high error values, indicating underfitting. On the contrary, those with truncation parameter values close to 135 present an increase

in their AICc, indicating a higher risk of overfitting. Those are them the extreme options that must be avoided.

For both discharge and efficiency, a 3-D visualization of four surrogate functions with different truncation parameters are also presented in Figures 6 and 7. These four options of surrogate function are presented with the superscripts ^{A}, ^{B}, ^{C} and ^{D}.

The surrogate functions $\hat{f}_Q^A$ and $\hat{f}_\eta^A$ have large deviations between their estimations and the available measurements and are an example of underfitting. The functions $\hat{f}_Q^B$ and $\hat{f}_\eta^B$ have enough Hermite polynomials to properly fit the measurements with low error, also featuring low AICc. The functions $\hat{f}_Q^C$ and $\hat{f}_\eta^C$ have the lowest AICc values, indicating no overfitting or underfitting. The functions $\hat{f}_Q^D$ and $\hat{f}_\eta^D$ exhibit an increase in AICc, and their 3-D visualizations made apparent non-realistic surface undulations for a typical discharge or efficiency function, clearly indicating data overfitting.

In fact, any surrogate function with truncation parameters comprised between the options ^{B} and ^{C} can be considered as a good approximation model. For this paper, the options $\hat{f}_Q^B$ and $\hat{f}_\eta^B$ are chosen, as the resulting errors are already small and increasing the complexity of the model would only lead to a negligible reduction in error. The functions $\hat{f}_Q^B$ and $\hat{f}_\eta^B$ are also presented through the isolines in the 2-D hill charts of Figures 8(a) and (b).

Using the surrogate functions $\hat{f}_Q^B$ and $\hat{f}_\eta^B$ and the measured values of α and P_a of the prototype, the prototype discharge and efficiency are estimated and the results are presented in Figure 9. From these results, E, Q_ED and n_ED are calculated and the resulting operating conditions are presented in the hill chart of Figure 10.

As the estimated values of prototype Q_ED and n_ED presented in Figure 10 illustrates, the tests started with the unit at very low discharge, so outside the rated operating range. The discharge is then increased and the unit enters in its rated range, but quickly moves into the cavitation zone. Two operating points are located at the limits of the rope-free zone. The two last ones, done at the highest discharge values, are outside the rated range and in a dangerous full

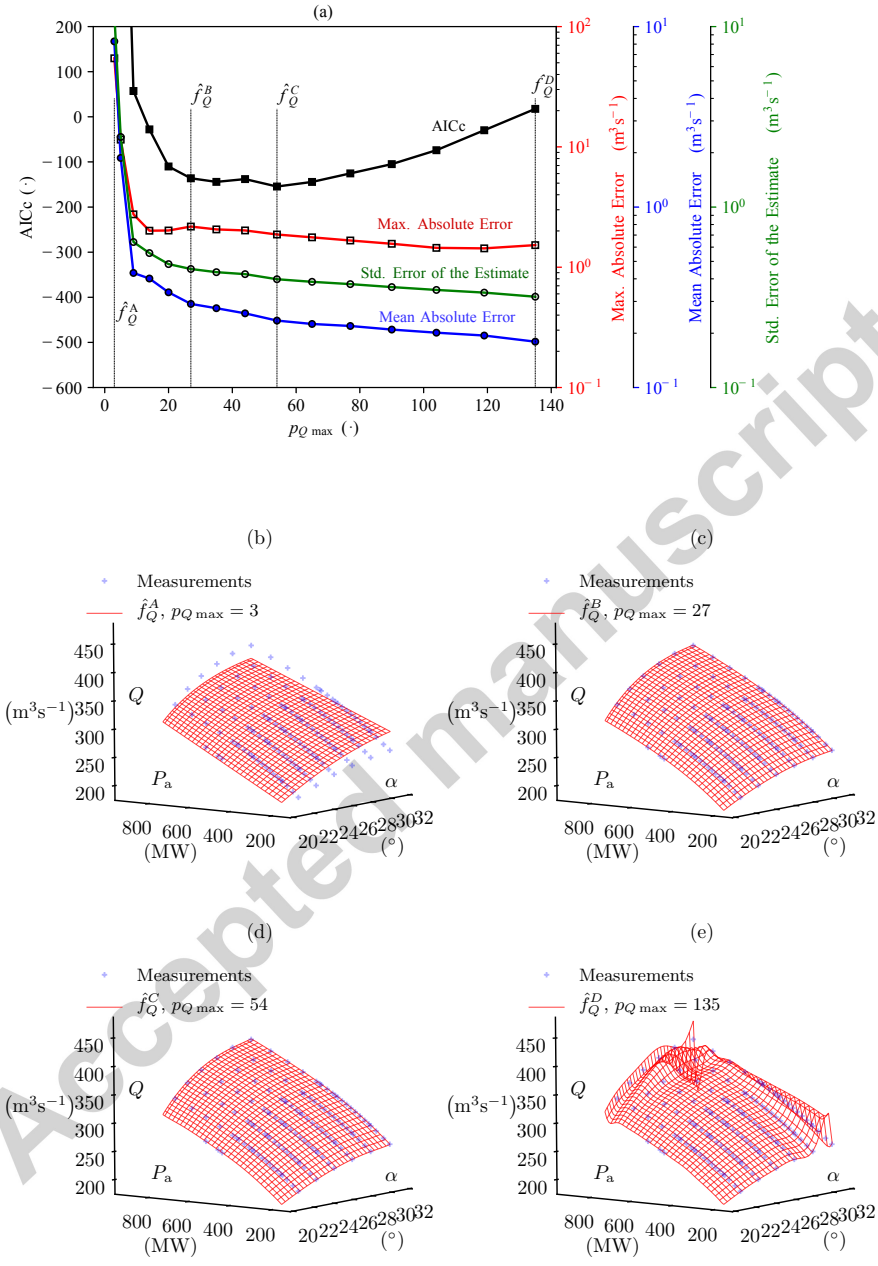

Figure 6: (a) AICc, maximum absolute error, mean absolute error and standard error for $p_{Q\,\max}$ values varying from 3 to 135. (b) Example of surrogate function underfitting the available points. (c) Surrogate function with the chosen $p_{Q\,\max}$ value. (d) Function with lowest AICc. (e) Function overfitting the points.

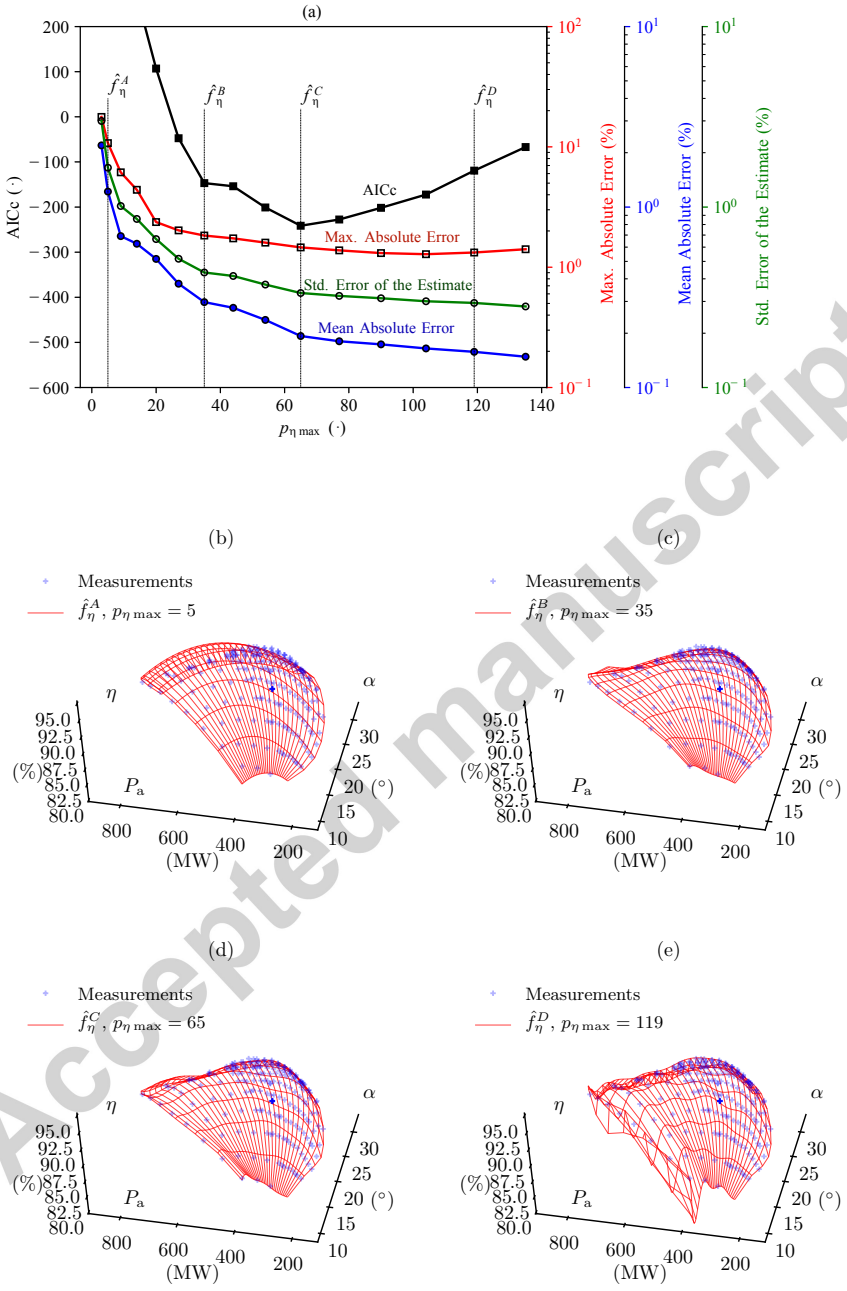

Figure 7: (a) AICc, maximum absolute error, mean absolute error and standard error for $p_{\eta\,\max}$ values varying from 3 to 135. (b) Example of surrogate function underfitting the available points. (c) Surrogate function with the chosen $p_{\eta\,\max}$ value. (d) Function with lowest AICc. (e) Function overfitting the points.

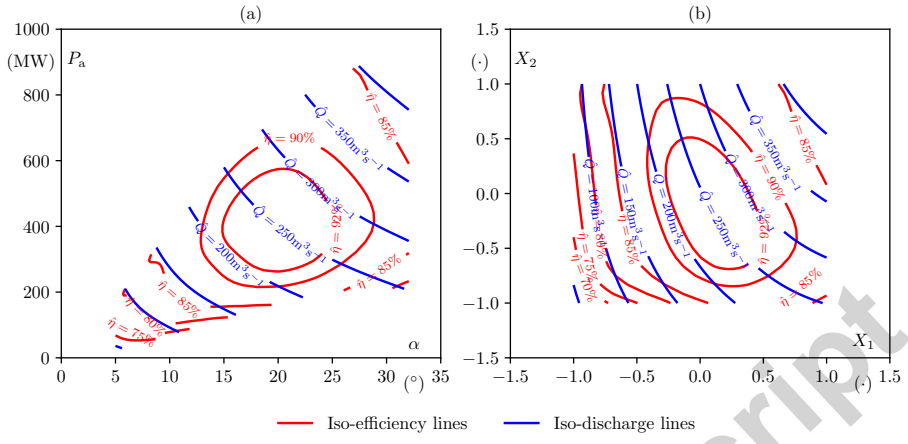

Figure 8: (a) Isolines of discharge and efficiency as a function of α and P_a and (b) as a function of X_1 and X_2.

load zone where a pulsating cavitation vortex rope may appear.

6. Validation

Because of the lack of direct measurement of the discharge, the method has been validated by comparing the gross head measured value with the gross head value resulting of the application of the present methodology. These two values are presented in Figure 11(a) and the error between them is shown in Figure 11(b)

The uncertainty bars shown in Figure 11 indicate the expected uncertainty using the methodology presented in this paper. It combines the following uncertainties:

- uncertainty on the discharge measurements performed on the reduced scale physical model equal to 0.10% of the maximum tested discharge;
- uncertainty on the efficiency measurements performed on the reduced scale physical model equal to 0.20%;

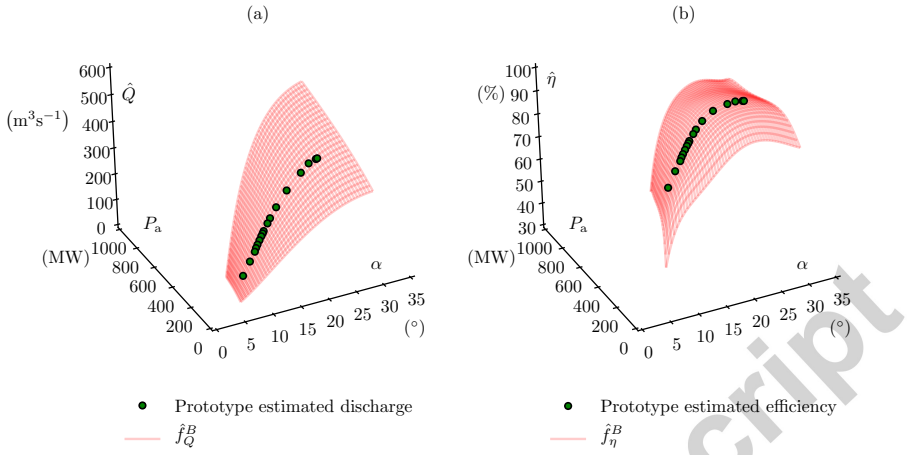

Figure 9: (a) Estimated values of discharge during the site tests and the surrogate function $\hat{f}_Q^B$ and (b) the estimated values of efficiency and $\hat{f}_\eta^B$.

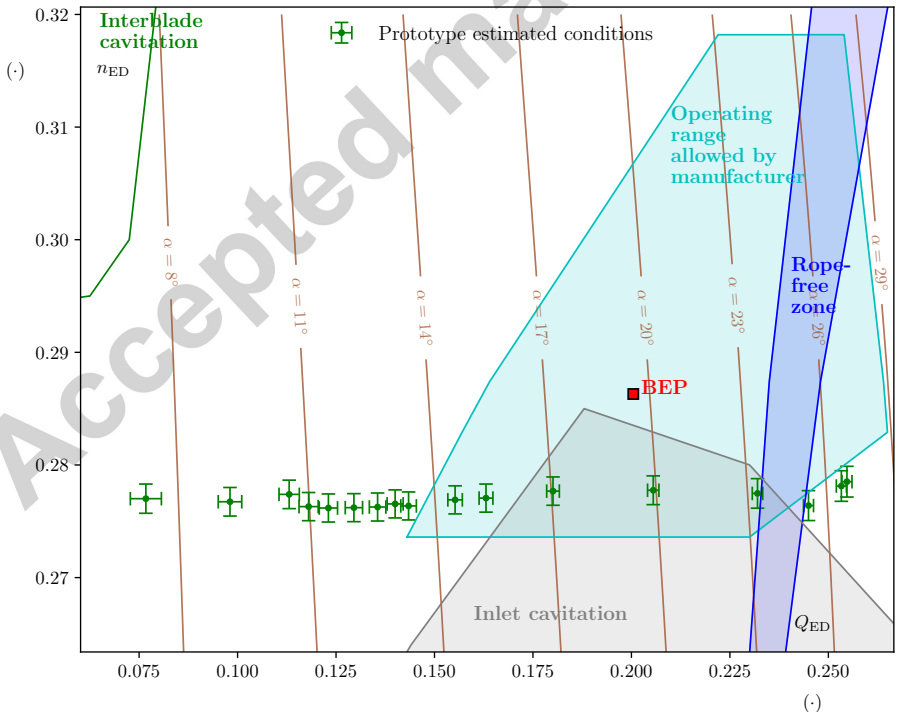

Figure 10: Estimated prototype operating conditions inside its hill chart

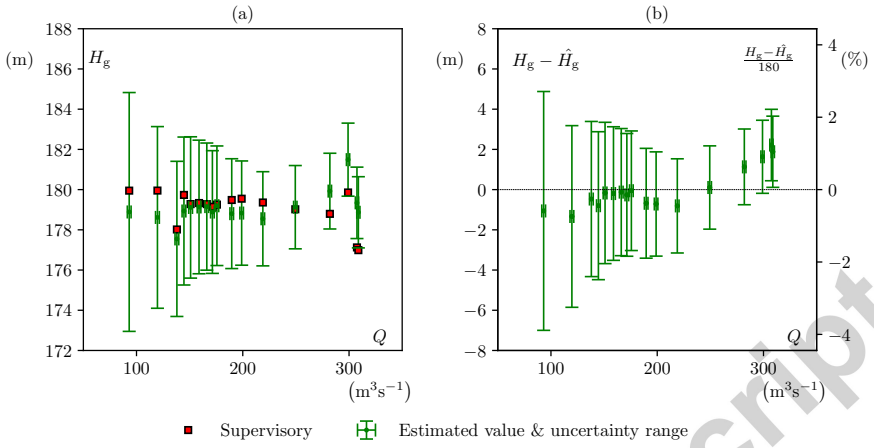

Figure 11: (a) Estimate gross head and the gross head recorded by the plant supervisory. (b) Error between the two values.

- uncertainty due to the polynomial approximation of the discharge and efficiency equal to the standard error of the estimate;
- uncertainty on the prototype active power measurement equal to 0.70% of the maximum tested power;
- uncertainty on the prototype guide vanes angle measurement equal to 0.18°, the standard error of the polynomial approximation .

A comparison between the expected uncertainty for the gross head estimates using the method presented in this paper and the expected uncertainty by doing direct measurements as described by the IEC standard [20] is presented in Figure 12. The presented expected uncertainty assuming the use of measurement methods in the IEC standard combine the following uncertainties:

- uncertainty on the discharge measurement equal to 1.70%, which is the expected measurement uncertainty on discharge measurements using the pressure-time method according to [20]);
- uncertainty on the prototype efficiency equal to 2.00%;

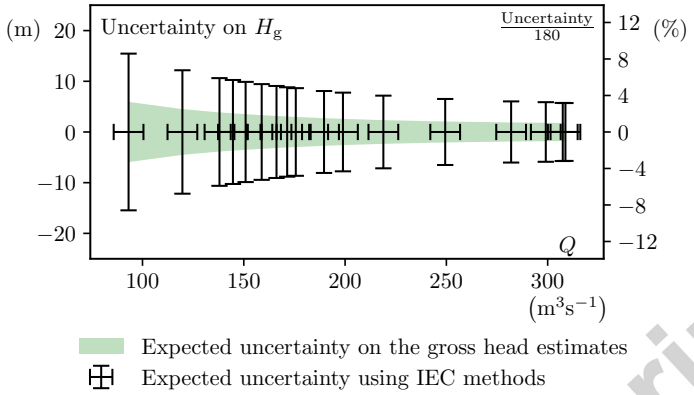

Figure 12: Comparison between the expected uncertainty using the method presented in this paper and the expected uncertainty by doing direct measurements as described by the IEC standard.

- uncertainty on the prototype active power measurement equal to 0.70% of the maximum tested power.

With the exception of the head calculated for the two highest values of discharge, all the head values provided by the supervisory are inside the calculated uncertainty range. The maximum difference between the calculated H_g and the one provided by the supervisory is of only 2.2 mwc, representing a relative error of 1.2 %. This low deviation value suggests that the estimated values $\hat{Q}$ and $\hat{\eta}$ during the tests on the prototype are accurate.

It can also be noticed by the comparison shown in Figure 12 that direct measurements described by the IEC standard could possibly lead to higher values of uncertainty. In reality, sources of uncertainties due to the transposition of the results from the model to the prototype were ignored and would increase the uncertainties of the estimations using the methodology presented in this paper. A deeper and thorough investigation of this type of error propagation is outside the scope of this paper.

7. Conclusions

A methodology to monitor the operating conditions of a Francis turbine prototype is presented. It is based on two inputs from the generating unit, the active power and the guide vanes opening angle, and data from tests on a homologous reduced scale physical model turbine.

A test case where a 444 MW turbine prototype is operating at 17 different operating conditions is presented. For these conditions, values for the turbine discharge, efficiency, available specific energy, IEC speed factor, IEC discharge factor and the plant gross head are estimated. The estimated gross head, which requires both the turbine discharge and the efficiency as input, is then compared to the gross head obtained through direct measurements, leading to a good agreement between measurements and calculations.

Comparisons between expected uncertainties using the presented methodology and the uncertainties while using typical direct measurements are presented. The uncertainty values on the presented estimations are expected to be relatively low if the uncertainties related to the measurements transposition from scaled model to prototype are ignored.

The results lead to the conclusion that in situations where direct measurements of discharge or efficiency on the prototype are not suitable and tests on the reduced scale physical model are available, the presented monitoring methodology provides a good estimation of the turbine operating conditions. Such information is of critical relevance to optimize the operation of a hydropower plant as it can help operators to avoid operating the unit outside the range specified by the manufacturer, avoid harsh cavitation conditions, search for the best total power dispatch scheme and consequently increase the overall annual hydraulic energy harnessing. Moreover, it can work in parallel to monitoring systems more focused on vibration or pressure pulsations, providing a larger picture of the prototype behavior.

Acknowledgements

The authors would like to thank BC Hydro (CA) for making available both the reduced scale physical model and the prototype generating unit for tests. In particular thanks to Danny Burggraeve, Jacob Losfin, and their staff. The authors would also like to acknowledge the commitment of the Laboratory for Hydraulic Machines technical staff, especially Raymond Fazan, David Buzzi, Georges Crittin, Alberto Bullani, Alain Renaud and Vincent Berruex.

Funding

The research leading to the results published in this paper is part of the HYPERBOLE research project, granted by the European Commission (ERC/FP7-ENERGY-2013-1-Grant 608532).

References

[1] A. Favrel, A. Müller, C. Landry, J. Gomes, K. Yamamoto, F. Avellan, Dynamics of the precessing vortex rope and its interaction with the system at francis turbines part load operating conditions, Journal of Physics: Conference Series 813 (1) (2017) 012023.
URL http://stacks.iop.org/1742-6596/813/i=1/a=012023

[2] A. Müller, A. Favrel, C. Landry, K. Yamamoto, F. Avellan, Experimental hydro-mechanical characterization of full load pressure surge in francis turbines, Journal of Physics: Conference Series 813 (1) (2017) 012018.
URL http://stacks.iop.org/1742-6596/813/i=1/a=012018

[3] U. Dorji, R. Ghomashchi, Hydro turbine failure mechanisms: An overview, Engineering Failure Analysis 44 (2014) 136 – 147. doi:https://doi.org/10.1016/j.engfailanal.2014.04.013.
URL http://www.sciencedirect.com/science/article/pii/S1350630714001277

[4] X. Liu, Y. Luo, Z. Wang, A review on fatigue damage mechanism in hydro turbines, Renewable and Sustainable Energy Reviews 54 (2016) 1–14.

[5] F. Avellan, Introduction to cavitation in hydraulic machinery, in: The 6th International Conference on Hydraulic Machinery and Hydrodynamics, Timisoara, Romania, 2004.

[6] R. Goyal, B. K. Gandhi, Review of hydrodynamics instabilities in francis turbine during off-design and transient operations, Renewable Energy 116 (2018) 697–709.

[7] P. Kumar, R. Saini, Study of cavitation in hydro turbines—a review, Renewable and Sustainable Energy Reviews 14 (1) (2010) 374–383.

[8] C. Valero, E. Egusquiza, A. Presas, D. Valentin, M. Egusquiza, M. Bossio, Condition monitoring of a prototype turbine. description of the system and main results, in: Journal of Physics: Conference Series, Vol. 813, IOP Publishing, 2017, p. 012041.

[9] E. C. Bortoni, G. S. Bastos, T. M. Abreu, B. Kawkabani, Online optimal power distribution between units of a hydro power plant, Renewable Energy 75 (2015) 30–36.

[10] M. Ak, E. Kentel, S. Savasaneril, Operating policies for energy generation and revenue management in single-reservoir hydropower systems, Renewable and Sustainable Energy Reviews 78 (2017) 1253–1261.

[11] Y. Shang, S. Lu, J. Gong, R. Liu, X. Li, Q. Fan, Improved genetic algorithm for economic load dispatch in hydropower plants and comprehensive performance comparison with dynamic programming method, Journal of Hydrology 554 (2017) 306–316.

[12] I. E. Commission, et al., Hydraulic turbines, storage pumps and pump-turbines — model acceptance tests, Standard No. IEC 60193, International Electrotechnical Commission, 1999.

[13] I. E. Commission, et al., Hydraulic machines, radial and axial – Performance conversion method from model to prototype, Standard No. IEC 62097, International Electrotechnical Commission, 2009.

[14] K. Yamamoto, A. Müller, A. Favrel, F. Avellan, Experimental evidence of inter-blade cavitation vortex development in francis turbines at deep part load condition, Experiments in Fluids 58 (10) (2017) 142. doi:10.1007/s00348-017-2421-z.
URL https://doi.org/10.1007/s00348-017-2421-z

[15] M. H. Stone, The generalized weierstrass approximation theorem, Mathematics Magazine 21 (5) (1948) 237–254.

[16] C. Hermite, Sur un nouveau développement en série des fonctions, Mallet-Bachelier, 1864.

[17] L. Andolfatto, J. Delgado, E. Vagnoni, C. Münch-Alligné, F. Avellan, Analytical hill chart towards the maximisation of energy recovery in water utility networks with counter-rotating runners micro-turbine, in: E-proceeding of the 36th IAHR World Congress 2015, The Hague, The Netherlands, 2015.

[18] H. Akaike, Problems of control and information, in: 2nd International Symposium on Information Theory, Budapest: Akademiai Kaido, 1973, pp. 267–281.

[19] C. M. Hurvich, C.-L. Tsai, Regression and time series model selection in small samples, Biometrika 76 (2) (1989) 297–307.

[20] I. E. Commission, et al., Field Acceptance Tests to Determine the Hudraulic Performance of Hydraulic Turbines, Storage Pumps and Pump-turbines, Standard No. IEC 60041, International Electrotechnical Commission, 1991.

[21] I. E. Commission, et al., Rotating electrical machines–Part 2-1: Standard methods for determining losses and efficiency from tests (excluding machines for traction vehicles), Standard No. IEC 60034-2-1, International Electrotechnical Commission, 2014.